

PAPER

Cite this: *J. Mater. Chem. A*, 2017, 5, 16722**Structural transformations in $\text{Li}_2\text{MnSiO}_4$: evidence that a Li intercalation material can reversibly cycle through a disordered phase†**Qing Chen,^{‡ab} Penghao Xiao,^{‡b} Yi Pei,^a Yan Song,^c Cheng-Yan Xu,^a Liang Zhen^{*a} and Graeme Henkelman^{‡*b}

$\text{Li}_2\text{MnSiO}_4$ is a promising high capacity cathode material due to the potential to extract two Li ions per formula unit. In practice, however, the use of $\text{Li}_2\text{MnSiO}_4$ is restricted by a low discharge capacity, which has been attributed to an irreversible structural change in the first charge cycle. In this work, we use density functional theory calculations to explore the details of this structural change, and our results reveal that the structural change during delithiation has two components. First, we find that the material undergoes a structural collapse upon partial delithiation, which is characterized by distortion of the MnO_4 tetrahedron. Remarkably, while this transformation results in a disordered structure, our calculations show that it is reversible upon relithiation and that the transformation does not strongly impede Li de/intercalation. The calculated reversibility of the phase change is consistent with recent experimental X-ray diffraction measurements showing that peaks associated with the crystalline MnO_4 order, which disappear upon delithiation, are restored upon lithiation. Additional experiments are conducted showing the reversibility of the material during cycling as a function of charging cutoff voltages. Second, we argue that, the irreversible structural degradation is primarily caused by oxygen evolution in the highly delithiated state; the oxygen deficient structure can only reincorporate half of the total Li when discharged to 1.5 V. Experimentally observed voltage profile shifts of $\text{Li}_2\text{MnSiO}_4$ during the first few cycles as well as the different electrochemical behavior exhibited by $\text{Li}_2\text{FeSiO}_4$ can be explained by this two-component structural change model.

Received 8th April 2017
Accepted 10th July 2017

DOI: 10.1039/c7ta03049e

rsc.li/materials-a

Introduction

Lithium transition metal silicate materials (Li_2MSiO_4 , M = Fe, Mn, Co, Ni) have been investigated as promising cathode materials in Li ion batteries due to their high theoretical capacity of *ca.* 330 mA h g^{-1} .¹ This high theoretical capacity, which corresponds to cycling two Li ions per formula unit (FU), cannot be achieved in Li_2MSiO_4 (M = Fe, Co, Ni) due to the limited electrochemical stability window of standard electrolytes. $\text{Li}_2\text{MnSiO}_4$ is the only member of the family from which the second Li ion can be theoretically extracted within the stable voltage window of existing electrolytes; it has hence attracted attention as a promising candidate for next generation cathodes in Li ion batteries. In

practice, however, $\text{Li}_2\text{MnSiO}_4$ provides only a low discharge capacity even in the first cycle, impeding the use of $\text{Li}_2\text{MnSiO}_4$.^{2–6} To explore the origin of the limited discharge capacity of $\text{Li}_2\text{MnSiO}_4$, XRD and TEM measurements were conducted to elucidate structural changes during the first charge/discharge cycle.^{7,8} It was found that the material loses its crystallinity when first charged to 4.4 V and is further converted into an amorphous state at 4.8 V. This latter electrochemically induced structural change is irreversible in that crystallinity is never recovered.⁸

Previous calculations based on density functional theory (DFT) have found that a highly delithiated structure undergoes a large volume contraction accompanied with a collapse of the initial layered framework.^{7,9–19} The collapse of the structure upon initial delithiation has become an accepted cause of the irreversible structural transformation that leads to the limited discharge capacity and poor cyclability of $\text{Li}_2\text{MnSiO}_4$. However, this argument is based on the volume change but not the energetics of the phases. The primary question addressed here is whether the collapsed LiMnSiO_4 structure can recover to the orthorhombic $\text{Li}_2\text{MnSiO}_4$ structure simply through voltage control and Li intercalation. Before addressing this specific point, we note that the possibility of a reaction within the time scale of interest is determined by whether the barrier can be

^aSchool of Materials Science and Engineering, Harbin Institute of Technology, Harbin 150001, China. E-mail: lzhen@hit.edu.cn

^bDepartment of Chemistry and the Institute for Computational Engineering and Sciences, The University of Texas at Austin, Austin, Texas 78712-0165, USA. E-mail: henkelman@utexas.edu

^cSchool of Materials Science and Engineering, Harbin Institute of Technology at Weihai, Weihai 264209, China

† Electronic supplementary information (ESI) available. See DOI: 10.1039/c7ta03049e

‡ These authors contributed equally to this work.

overcome at a given temperature. Here, the barriers for Li intercalation into the collapsed structure and the phase transition between the collapsed and the orthorhombic structure are needed to evaluate the discharge reversibility.

Recent experiments^{20–24} have provided a different picture of $\text{Li}_2\text{MnSiO}_4$ than previous reports that $\text{Li}_2\text{MnSiO}_4$ suffers from an irreversible amorphous transition in the first cycle.^{25,26} Instead, it is found that when half of the Li is extracted during the first charge (delithiation), the XRD peaks completely disappear, but surprisingly, the XRD peaks recover upon discharge (relithiation).^{20–22} This observation of reversibility shows that the structural change induced by partial delithiation is different from the irreversible change induced by complete delithiation. Thus, the traditional irreversible-collapse model is unable to explain the electrochemical behavior of $\text{Li}_2\text{MnSiO}_4$, and the connections to structural collapse and irreversible structural transformations need to be reconsidered.

In this work, we investigate the barriers of the structural evolution of $\text{Li}_2\text{MnSiO}_4$ during the de/lithiation process and the corresponding electrochemical behavior using DFT calculations. Remarkably, we find that the structural recovery from collapse upon full lithiation has a similar barrier to the structural collapse at half delithiation. Li intercalation in the collapsed structure has a very small barrier at low Li concentration and a large barrier at a high Li percentage. The latter barrier, however, is comparable to that in the fully lithiated orthorhombic structure, indicating that the cathode material can be operated reversibly, or at least that the cyclability is not reduced by the initial structural change. Finally, motivated by the fact that oxygen loss is known to cause capacity fade in layered LiCoO_2 (ref. 19, 27 and 28) and lithium rich^{29–31} materials, the possibility of oxygen evolution is examined for $\text{Li}_2\text{MnSiO}_4$ at various stages of delithiation. Our results indicate that the irreversible transition of $\text{Li}_2\text{MnSiO}_4$ is caused by oxygen evolution in the highly delithiated state, rather than the structural collapse which occurs at partial delithiation.

To verify the mechanism proposed here and to prove that the structural transition when charged below 4.4 V is reversible, cycling experiments and *ex situ* XRD were performed on $\text{Li}_2\text{MnSiO}_4$. We find, from the electrochemical performance in the first fifty cycles, that the capacity loss is aggravated by charging to a highly delithiated state. From our theoretical model, we can also explain the electrochemical behavior, including the cycling performance and coulombic efficiency, exhibited by $\text{Li}_2\text{FeSiO}_4$.^{32–34}

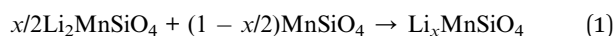
Computational details

Calculations based on DFT were performed using a plane wave basis set with the projector augmented wave framework³⁵ describing the core electrons, as implemented in the Vienna *ab initio* simulation package.³⁶ The exchange-correlation energy was evaluated within the generalized gradient approximation with a Hubbard U correction following the rotationally invariant form.³⁷ An effective U value of 4 eV ($J = 1$ eV) was used for the d-states of the transition metals. The energy cut-off for the plane wave basis set was 520 eV. The Monkhorst–Pack method was used to sample the Brillouin-zone with a k -point mesh of 6×6

$\times 6$. Structural optimization was continued until the force on each atom was less than $0.01 \text{ eV } \text{Å}^{-1}$. All structures were fully relaxed in terms of both cell parameters and atomic positions.

The orthorhombic $\text{Li}_2\text{MnSiO}_4$ with space group $Pmn2_1$ is the most stable fully lithiated structure. Various Li-vacancy arrangements were then tested to determine the most stable structure of $\text{Li}_x\text{MnSiO}_4$ as a function of Li content, x . LiMnSiO_4 and $\text{Li}_2\text{MnSiO}_4$ structures with a collapsed framework were obtained by inserting Li into the collapsed MnSiO_4 structure. The reversibility of the structural collapse was evaluated by calculating the transition barrier from the collapsed $\text{Li}_2\text{MnSiO}_4$ structure back to the orthorhombic structure using the solid-state nudged elastic band method.³⁸ The possibility of oxygen evolution was evaluated by calculating the formation energy of oxygen vacancies both in the unit cell and in a $1 \times 2 \times 2$ supercell. Li diffusion barriers at different delithiated states were calculated in a $2 \times 2 \times 2$ supercell.

To explore the structural evolution upon delithiation, we first find the most stable structure of $\text{Li}_x\text{MnSiO}_4$ as a function of Li concentration, x . The relative stability of $\text{Li}_x\text{MnSiO}_4$ ($0 \leq x \leq 2$) is compared by constructing a convex hull with formation energies evaluated as:



$$\Delta E = E - [x/2E_{\text{Li}_2\text{MnSiO}_4} + (1 - x/2)E_{\text{MnSiO}_4}], \quad (2)$$

where E is the total energy of $\text{Li}_x\text{MnSiO}_4$, $E_{\text{Li}_2\text{MnSiO}_4}$ is the total energy of the fully lithiated phase and E_{MnSiO_4} is the energy of the fully delithiated structure. Sixty different Li-vacancy configurations of LiMnSiO_4 in a $2 \times 2 \times 2$ supercell were examined.

Results and discussion

Reversible structural collapse

Fig. 1 shows the calculated convex hull of the material as a function of Li composition, as well as the three stable

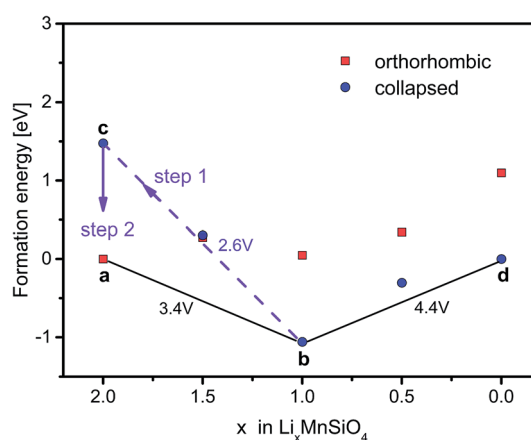


Fig. 1 Calculated convex hull of $\text{Li}_x\text{MnSiO}_4$ and the equilibrium voltages for de/lithiation.

Table 1 Calculated lattice parameters of $\text{Li}_x\text{MnSiO}_4$ ($x = 2, 1, 0$) during delithiation

	a (Å)	b (Å)	c (Å)	α (deg)	β (deg)	γ (deg)	Volume (Å ³)	Bonded Mn–O
$\text{Li}_2\text{MnSiO}_4$	6.37	5.45	5.05	90.00	90.00	90.00	175.13	4
LiMnSiO_4	6.30	5.17	5.21	74.52	88.19	99.52	160.60	5
MnSiO_4	6.38	5.74	4.45	67.44	89.98	102.29	146.49	5

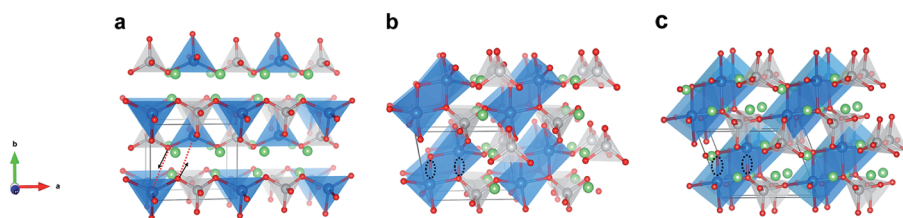


Fig. 2 The crystal structures of the three points (a, b, and c) from the convex hull in Fig. 1, (a) orthorhombic- $\text{Li}_2\text{MnSiO}_4$, (b) collapsed- LiMnSiO_4 and (c) collapsed- $\text{Li}_2\text{MnSiO}_4$. Atomic coloring is as: blue polyhedra are Mn; gray polyhedra are Si; green spheres are Li; and red spheres are O.

structures lying on the hull at $x = 2, 1, 0$, labeled a, b, and d, respectively. The lattice parameters of the three stable structures on the convex hull are shown in Table 1. When half of the total Li is removed, the framework has a volume contraction of 8.6%, and this contraction increases to 16.4% at full delithiation, accompanied by a significant distortion from orthogonal lattice angles. The corresponding crystal structures are displayed in Fig. 2. The most stable orthorhombic structure of $Pmn2_1$ $\text{Li}_2\text{MnSiO}_4$ is a layered framework with connected MnO_4 and SiO_4 tetrahedra lying on the horizontal plane. Unlike layered $\text{Li}_2\text{MnSiO}_4$, the most stable structure of LiMnSiO_4 and MnSiO_4 is the one that converts to a collapsed framework by connecting two tetrahedrons from the neighboring layers to form edge sharing MnO_5 square pyramids. The energy of this structure is calculated to be lower than those of other configurations, including the Li/Mn anti-site defect structure of LiMnSiO_4 . Although this collapsed structure is related to the crystallinity loss observed during the charge process in experiments, we find that the structure is not completely disordered but rather of a low triclinic symmetry.

The driving force of the structural change is that the most stable crystal field for Mn^{2+} and Mn^{3+} is a four-fold coordinated tetrahedron and a five-fold coordinated square pyramid, respectively.¹⁸ The attraction of Mn^{3+} to the extra O ion in the adjacent layer stabilizes the square pyramid structure.

Since $x = 1$ in $\text{Li}_x\text{MnSiO}_4$ is the point at which the structural collapse initiates, we focus on lithiation states from $x = 1$ to 2. The discharge process is separated into two steps for a simplified analysis: the first step is to insert Li back into the collapsed LiMnSiO_4 to form a collapsed $\text{Li}_2\text{MnSiO}_4$ and the second step is the phase transition from the collapsed $\text{Li}_2\text{MnSiO}_4$ to the orthorhombic layered $\text{Li}_2\text{MnSiO}_4$. As shown in Fig. 1, the collapsed $\text{Li}_2\text{MnSiO}_4$ is higher in energy than the layered one, which results in a discharge voltage that is 0.8 V lower than the charge voltage. The voltage to reach the collapsed $\text{Li}_2\text{MnSiO}_4$ structure, of 2.6 V, is within the electrolyte voltage window. We

also find that Li diffusion in the collapsed framework is no more difficult than that in the layered structure. Therefore, there is no additional energy barrier in the first step of Li intercalation into the collapsed structure compared to the initial delithiation process. If the second step, the phase transformation, is kinetically accessible at room temperature, the discharge will follow the black b–a line in Fig. 1 with a voltage of 3.4 V if discharged from b; otherwise the first discharge and all subsequent charge/discharge cycles will follow the purple b–c line in Fig. 1, with a voltage of 2.6 V. In either case, the extracted Li can be reinserted, indicating that the full discharge capacity of the material is theoretically accessible.

The calculated phase transition barrier from the collapsed $\text{Li}_2\text{MnSiO}_4$ to the orthorhombic layered structure is 0.12 eV per FU, as shown in Fig. 3. The five intermediate structures (a, b, c, d, and e) along the minimum energy pathway of the structural recovery is given in Fig. S1.† The barrier of the structural collapse in LiMnSiO_4 is 0.1 eV per FU, which is comparable to that of the recovery transition. Since the collapse occurs spontaneously when

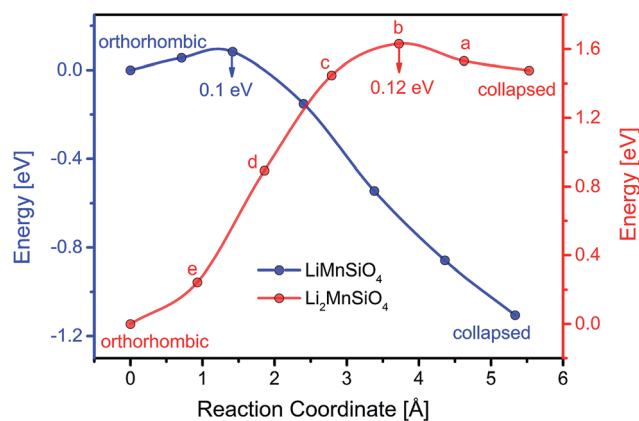


Fig. 3 Minimum energy pathways for the transition from the collapsed $\text{Li}_2\text{MnSiO}_4$ to the orthorhombic structure and from the orthorhombic LiMnSiO_4 to the collapsed structure.

half delithiated, the recovery to the orthorhombic layered structure when fully lithiated is not expected to be kinetically hindered. Thus, the two-step mechanism described above is shown to be both thermodynamically favorable and kinetically accessible. Actually, there can be many different reaction paths from a given initial to a final state; although our calculated path may not be the one with the lowest barrier, it does give an upper bound on the barrier, and clearly shows that the collapsed LiMnSiO_4 structure is able to transform back to the orthorhombic $\text{Li}_2\text{MnSiO}_4$ structure upon lithiation.

A reversible framework collapse should not be too surprising; other cathode materials have been shown to have a similar behavior. The Prussian blue analog $\text{Na}_2\text{FeMn}(\text{CN})_6$, for example, undergoes a monoclinic to rhombohedral phase transition with a significant volume contraction of 27% upon Na intercalation, and yet maintains excellent cyclability.³⁹ Important evidence supporting our calculation results can be found in a recent study by Moriya *et al.*²² In their experiment, $\text{Li}_2\text{MnSiO}_4$ was cycled to 1.25 Li per FU with 0.75 Li remaining in the material at the end of charging. From synchrotron-based X-ray analysis, some diffraction peaks were found to disappear or become markedly weaker after the first-charge which was attributed to local distortions of the MnO_4 tetrahedron with a pair distribution-function (PDF) analysis; however, following the first-discharge, the missing diffraction peaks reappear. The samples that were delithiated to a state of $\text{Li}_{0.75}\text{MnSiO}_4$ – corresponding to the collapsed structure in our calculations – exhibited excellent cyclability without irreversible capacity loss in the first cycle. This experimental observation strongly supports our claim that the collapsed structure can recover to the orthorhombic structure upon lithiation.

To provide additional support for our theoretical results, we have conducted experiments designed specifically to address the mechanism of capacity loss as a function of charging voltage in $\text{Li}_2\text{MnSiO}_4$. The synthesis method, morphology and XRD pattern of carbon coated $\text{Li}_2\text{MnSiO}_4$ are shown in the ESI.† Two sets of $\text{Li}_2\text{MnSiO}_4$ electrodes are compared, one charged to 4.2, 4.3, 4.4 and 4.5 V, and the other discharged to 1.5 V after charging to 4.2, 4.3, 4.4 and 4.5 V, respectively; the samples are marked as a, b, c, d, a', b', c' and d'. The *ex situ* XRD patterns and charge–discharge curves of each specimen are shown in Fig. 4. One can see that the reflections of $\text{Li}_2\text{MnSiO}_4$ gradually diminish and become almost undetectable when $\text{Li}_2\text{MnSiO}_4$ is charged to 4.4 V, indicating the loss of crystallinity with the extraction of Li. But when the electrode, that was charged to 4.4 V, is subsequently discharged with 1.1 Li per FU (Li reinserted into the material), the reflections of $\text{Li}_2\text{MnSiO}_4$ reappear in c', demonstrating the recovery of the orthorhombic ($Pmn2_1$) symmetry and that the collapse of LiMnSiO_4 is reversible. This phenomenon, which has also been shown in recent reports,^{20–22} is inconsistent with the traditional view that the crystallinity loss is irreversible. It should also be noted that there are no reflections in the pattern of d', suggesting that the recovery of symmetry is associated with partially delithiated states and would not occur upon high delithiation.

It is also interesting that even though the as-prepared $\text{Li}_2\text{MnSiO}_4$ is a pure phase, there appears to be some small additional peaks in the XRD pattern of the sample charged to 4.2 and 4.3 V. These reflections, which also appeared during the charging process, have been detected previously by both *in situ* and *ex situ* XRD measurements,^{21,40–42} yet no convincing interpretation of these peaks has been given. Based on our present

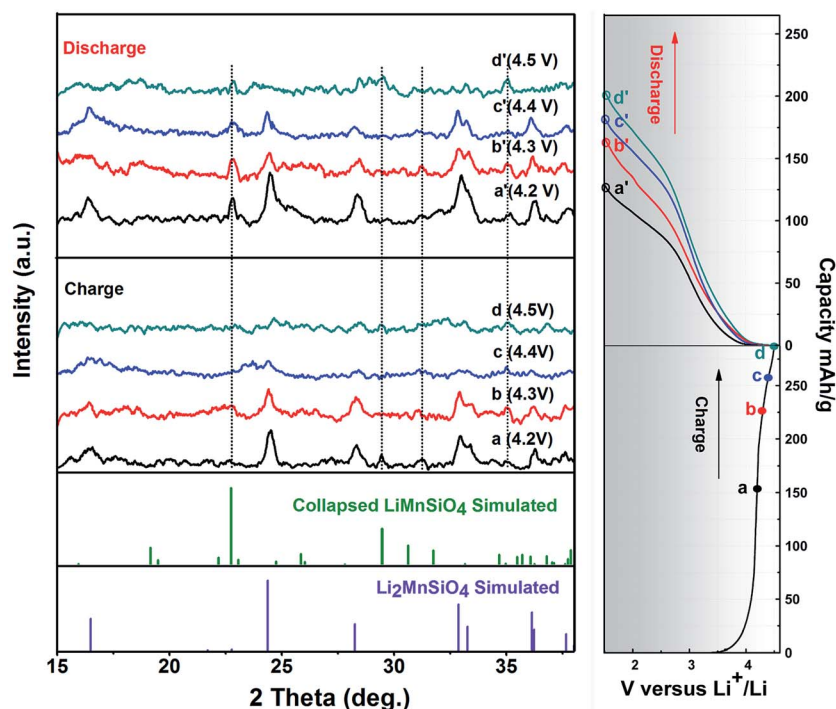


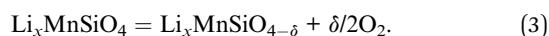
Fig. 4 *Ex situ* XRD patterns and charge–discharge curves of each specimen of $\text{Li}_2\text{MnSiO}_4$ which is charged to 4.2, 4.3, 4.4 and 4.5 V, respectively; and then discharged to 1.5 V.

calculations, these reflections can be indexed to the diffraction peaks of the collapsed structure of $\text{Li}_x\text{MnSiO}_4$ ($1 < x < 2$) which is distorted but retains some degree of long-range order. While it is difficult to identify the exact structure of this $\text{Li}_x\text{MnSiO}_4$ phase, we can compare the simulated Bragg peaks from the (theoretically) completely collapsed LiMnSiO_4 with the experimental peaks. As shown in Fig. 4, while there remain some deviations, most of the additional peaks in a and b can be assigned to the reflections in the simulated result, indicating that the additional phase possibly has a similar symmetry to collapsed LiMnSiO_4 . There are also additional peaks in the patterns of a', b' and c'. Although the intensity of reflections in the discharge group is different from that in the charged group, the positions are the same, suggesting the existence of the additional phase with a similar symmetry to collapsed LiMnSiO_4 . According to our model, the collapsed structure should transform to the initial orthorhombic structure under equilibrium; the coexistence of both phases in the discharged material may be due to incomplete lithiation in the discharge process because of the low lithium conductivity of $\text{Li}_2\text{MnSiO}_4$.

In summary, the crystallinity loss caused by the structural collapse in LiMnSiO_4 is theoretically reversible, as is confirmed by recent measurements^{20–22} and our experiments. Then one question remains: what structural change occurs at high delithiation which gives rise to the irreversible transition in the first cycle? Understanding this critical factor is key to improving the electrochemical performance of $\text{Li}_2\text{MnSiO}_4$.

The impact of oxygen evolution on electrochemical properties

It is widely reported that irreversible structural changes are accompanied by oxygen evolution in layered LiCoO_2 (ref. 19, 27 and 28) and Li-rich^{30,31} materials. Following this literature, we calculate the oxygen vacancy formation energy in $\text{Li}_x\text{MnSiO}_4$ from the Gibbs free energy of the following reaction at various Li charge states, x ,



where δ is the fraction of oxygen vacancies in the $\text{Li}_x\text{MnSiO}_4$ structure. For this calculation we considered two concentrations of oxygen vacancies (3.125 at% and 12.5 at%) for each state on the convex hull in Fig. 1. Different vacancy sites were examined to find the lowest energy configuration. The reaction enthalpy was calculated according to

$$\Delta H = \frac{E(\text{Li}_x\text{MnSiO}_{4-\delta}) + 0.5\delta E(\text{O}_2) - E(\text{Li}_x\text{MnSiO}_4)}{0.5\delta} \quad (4)$$

where E is the calculated energy of the indicated structure, per FU. Taking into account the entropy of O_2 in the standard state ($-T\Delta S = -0.63$ eV),⁴³ the Gibbs free energy ΔG is calculated from the reaction enthalpy. Fig. 5 shows the ΔG values of oxygen evolution at various Li charge states, for both vacancy concentrations considered. The vacancy formation energies are calculated to be positive in the Li rich phase, $\text{Li}_x\text{MnSiO}_4$ ($x \geq 1$), and negative in Li poor phases, $\text{Li}_{0.5}\text{MnSiO}_4$ and MnSiO_4 . This calculation indicates that oxygen evolution is thermodynamically favorable in the highly delithiated phase and that O_2 could

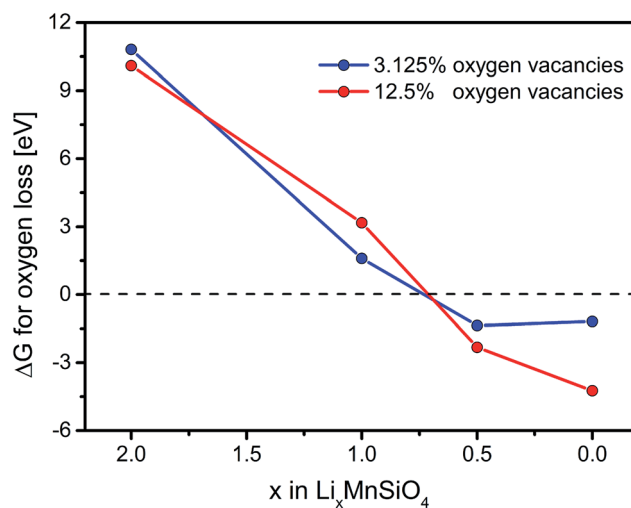


Fig. 5 Calculated Gibbs free energy for O_2 release as a function of lithiation, x , in $\text{Li}_x\text{MnSiO}_4$, based on two concentrations of oxygen vacancies.

be released from the cathode,⁴⁴ for example by reacting with the organic electrolyte or by other irreversible mechanisms. In fact, oxygen evolution in the highly delithiated state is not surprising. When Li atoms are extracted from the material, charge neutrality of the system is maintained by the oxidation of the transition metal redox couple, $\text{Mn}^{2+}/\text{Mn}^{3+}$. In the highly delithiated state, to compensate for the system charge, the material is more prone to anionic redox reactions in the form of oxygen evolution than an increase in the oxidation state of the transition metal to Mn^{4+} . A previous *in situ* XAS experiment of $\text{Li}_2\text{MnSiO}_4$ showed no indication of Mn^{4+} upon cycling,⁴⁵ which provides evidence of the reduction of Mn^{4+} to Mn^{3+} by oxygen evolution. A direct experimental verification of O_2 release could be performed by either operando mass spectrometry or differential electrochemical mass spectrometry.^{46,47}

The redox activity of oxygen in $\text{Li}_2\text{MnSiO}_4$ during Li extraction can be understood from the calculated density of states (DOS). Fig. S3† shows the total DOS of $\text{Li}_2\text{MnSiO}_4$ and partial densities obtained by atomic projections of the Mn-3d and O-2p states. $\text{Li}_2\text{MnSiO}_4$ is an insulator with a band gap over 3 eV. The bottom of the conduction band is dominated by Mn-3d states. Upon delithiation, the Fermi level moves into the valence band. When delithiated to $\text{Li}_{0.5}\text{MnSiO}_4$, the band in the vicinity of the Fermi level is primarily of O-2p character, consistent with the predominantly anionic redox character found in Li_2MnO_3 .⁴⁸ The facile formation of holes in the O-2p band explains the spontaneous oxygen evolution in $\text{Li}_{0.5}\text{MnSiO}_4$.

To explore the effects of oxygen evolution on the charge/discharge process, structures with oxygen loss have been added to the convex hull, as shown in Fig. 6. The formation energy of these structures is calculated as the energy change of the reaction,



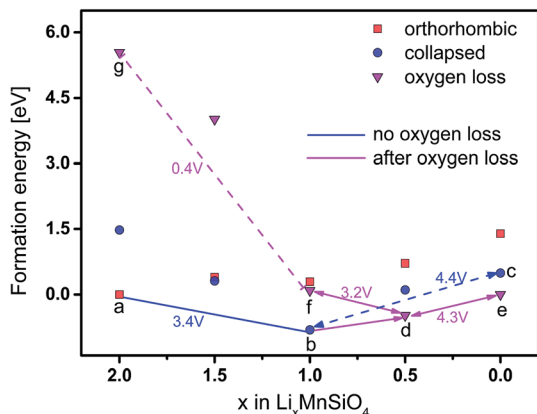


Fig. 6 Revised convex hull considering structures containing 12.5% oxygen vacancies.

Although O_2 gas is released in this reaction, the formation energies for oxygen deficient phases in Fig. 6 are calculated with respect to the energy of stoichiometric $\text{Li}_x\text{MnSiO}_{4-\delta} + \delta/2\text{O}_2$, which makes the relative stability of stoichiometric and oxygen deficient structures directly comparable.

In Fig. 6, points b and c are collapsed structures with no oxygen loss; points d and e are collapsed structures with 12.5% oxygen vacancies. Since the calculated Gibbs free energy of 12.5% oxygen vacancies is lower than that of 3.125%, the thermodynamic equilibration for oxygen evolution is not achieved until 12.5% oxygen has been lost. Thus, it makes sense to discuss the effect of oxygen evolution under the greater, 12.5%, concentration of oxygen vacancies.

The four points (a, b, d, and e) lying on the hull indicate that the structure undergoes a collapse transformation when $x \leq 1$, and then oxygen evolution when $x \leq 0.5$. Since the oxygen vacancies are retained in subsequent cycles, the process of discharging follows $e \Rightarrow d \Rightarrow f \Rightarrow g$, along the magenta lines in Fig. 6. The formation energy of point g is excessively high, resulting in a voltage of 0.4 V from f to g, which is too low for cathode materials, and thus prohibits the complete lithiation to $\text{Li}_2\text{MnSiO}_{4-\delta}$. The accessible discharge path of the material with a small amount of oxygen loss is $e \Rightarrow d \Rightarrow f$, and subsequent

cycles follow $e \Leftrightarrow d \Leftrightarrow f$. By contrast, if there is no oxygen loss during delithiation, the charge/discharge cycles follow the blue lines $a \Leftrightarrow b \Leftrightarrow c$. We hence propose that oxygen evolution would contribute to the irreversible capacity loss: the oxygen deficient structure impedes the second Li insertion from $\text{LiMnSiO}_{4-\delta}$ to $\text{Li}_2\text{MnSiO}_{4-\delta}$, resulting in half of the theoretical capacity loss in the first cycle. An experiment by Kokalj⁷ supports this mechanism, in which the parent $\text{Li}_2\text{MnSiO}_4$ and the material formed after one completed charge–discharge cycle were examined using Li MAS NMR spectroscopy; the results showed that the composition of the cycled material was approximately $\text{Li}_{0.8}\text{MnSiO}_4$.

Voltage profiles can reflect structural stability; shifts in a voltage plateau indicate a phase transition to a different structure. Fig. 7a shows the calculated voltages of the delithiated structure. In the first cycle, the voltage for extracting half of the Li would be 3.4 V in equilibrium. Here, equilibrium means that the charging rate is slow enough that the delithiated component can relax to the lowest energy structure lying on the convex hull. The second half-Li per FU is then extracted at 4.4 V ($b \Leftrightarrow c$) and would remain constant in subsequent cycles if there were no oxygen loss. Since the host structure transforms to $\text{MnSiO}_{4-\delta}$, the discharge process and subsequent cycles have two shorter plateaus at 4.3 V ($d \Leftrightarrow e$) and 3.2 V ($f \Leftrightarrow d$). The shifts of these plateaus, considering the oxygen loss mechanism, are a good match to the experimental cyclic voltammogram measurements⁴⁹ (at 25 °C and a scan rate of 0.05 mV s^{-1}). In the first charging process, as shown in Fig. 7b, only one broadened cathodic peak located at 4.5 V has been detected, which may be influenced by polarization effects and side reactions. Open circuit voltages at different depths of charge (with cut-off voltages of 3.7 and 4.2 V, respectively) suggest that the equilibrium potential of LiMnSiO_4 vs. Li is near 3.3 V, which is in accordance with our calculations. In subsequent cycles, the cathodic reaction peak shifts to lower voltage and splits into two peaks located at 4.3 and 4.5 V. Since the anodic peaks of the first three cycles are almost the same, the shift of the cathodic peaks indicates that oxygen evolution in the first charging process may lower the reaction potential in subsequent cycles.

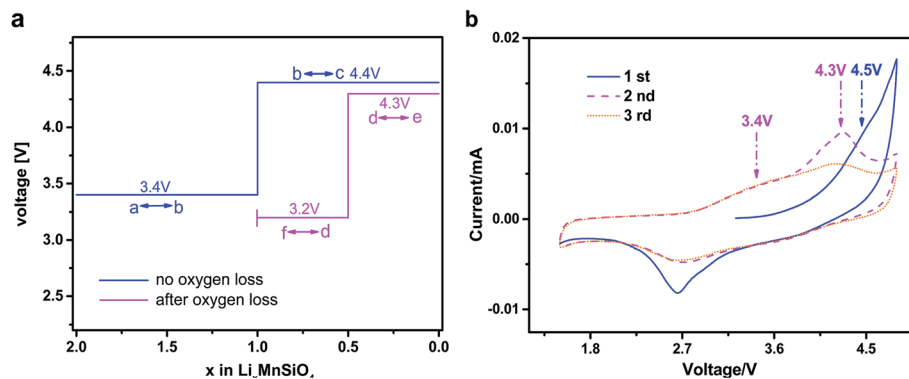


Fig. 7 (a) Calculated equilibrium voltage with and without oxygen loss (the concentration of oxygen vacancy is 12.5%). (b) Experimental cyclic voltammograms of $\text{Li}_2\text{MnSiO}_4$ for the first three cycles (at 25 °C and a scan rate of 0.05 mV s^{-1}).⁴⁹

From the considerations presented here, we can conclude that the irreversible structural change in the first charge process is primarily caused by oxygen evolution rather than structural collapse. Oxygen evolution not only prevents the high reversible capacity, but also gives rise to the poor cyclic performance of $\text{Li}_2\text{MnSiO}_4$. Specific experiments on the cycle performance of $\text{Li}_2\text{MnSiO}_4$ over various voltage regions (Fig. S4†) are performed to support this claim. The capacity fade is significantly accelerated in samples with initial discharge capacities of more than 250 mA h g^{-1} , corresponding to a Li extraction of more than 1.5 per formula unit. These data indicate that the deteriorated cyclic performance of $\text{Li}_2\text{MnSiO}_4$ is primarily due to the oxygen loss at high states of delithiation. Although the poor cycling at high voltages may also be influenced by electrolyte oxidation, which is difficult to eliminate,⁴⁶ the degradation of capacity retention observed here is significantly larger than what would be expected from interference phenomena including electrolyte oxidation.

Comparison to $\text{Li}_2\text{FeSiO}_4$

Interestingly, within the same family of transition metal silicates, $\text{Li}_2\text{FeSiO}_4$ polymorphs can only extract one Li per FU below 4.8 V and exhibit good cyclability only if the charge voltage is kept below 4.8 V.^{32–34} However, $\text{Li}_2\text{FeSiO}_4$ also undergoes a significant phase transformation from the monoclinic to the orthorhombic structure upon the first charge to a half-delithiated structure, as well as showing significant Li/Fe anti-site mixing in the following cycles.⁵⁰

The model that we have described should be able to explain this difference. Accordingly, we performed the same calculations to construct the convex hull of $\text{Li}_x\text{FeSiO}_4$. To consider the Li/Fe anti-site defects in LiFeSiO_4 , we employed the basin-hopping algorithm to search for the global minimum configuration based on a $1 \times 1 \times 2$ supercell, and found that Fe ions would spontaneously migrate towards Li vacancies. With 12.5% oxygen vacancies in $\text{Li}_x\text{FeSiO}_4$ ($x = 1, 0$), the Gibbs free energy change was calculated to be -2.1 eV in the fully delithiated structure, indicating that the material would release oxygen spontaneously if all the Li could be extracted from the host. In fact, oxygen redox in highly charged $\text{Li}_2\text{FeSiO}_4$ has been predicted by other DFT calculations, where the formation of holes in the O-2p band was found when more than one Li per FU was extracted.⁵¹

Fig. 8 shows the calculated convex hull considering 12.5% oxygen vacancies contained in high delithiated structures and the corresponding delithiation voltage. The first delithiation voltage is 2.8 V, in agreement with that of the $Pmn2_1$ structure measured in experiments;³² the second delithiation voltage is 4.8 V, if oxygen evolution is not sufficiently rapid, which is close to the electrolyte decomposition voltage. This is the most significant limitation for the application of $\text{Li}_2\text{FeSiO}_4$ as the second Li cannot be extracted due to the excessive voltage required. Therefore, in most experiments, $\text{Li}_2\text{FeSiO}_4$ can only cycle in the range $1 \leq x \leq 2$ (solid line in Fig. 8) which is energetically unfavorable for oxygen evolution. We also note that the second-electronic process gives rise to a high charge

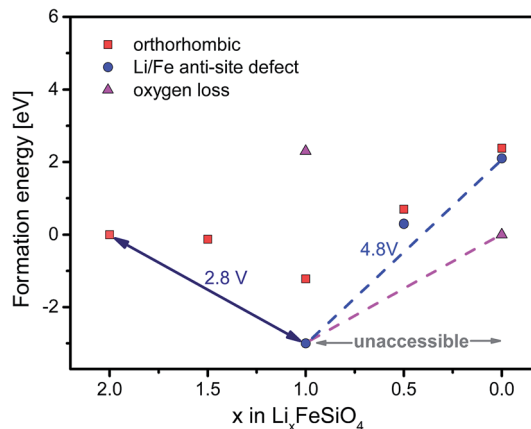


Fig. 8 Calculated convex hull of $\text{Li}_x\text{FeSiO}_4$ considering 12.5% oxygen vacancies contained in high delithiated structures and the corresponding delithiation voltage.

capacity of close to 300 mA h g^{-1} in $\text{Li}_2\text{FeSiO}_4$,⁵² and the relatively large discharge capacity loss is inevitable compared to the completely reversible capacity of one Li extraction/insertion cycle.⁵⁰

Thus, we can conclude that during charge/discharge the structural collapse in $\text{Li}_2\text{MnSiO}_4$, due to the distortions of the MnO_4 tetrahedron, as well as the structural change in $\text{Li}_2\text{FeSiO}_4$, *i.e.* the formation of so-called Li/Fe anti-site defects, will not necessarily result in irreversible cycling of the materials. It is the oxygen evolution at highly charged states that causes the irreversible structural change. If more than one and a half Li per FU are extracted, oxygen evolution will occur in both materials. The crucial difference between them is that $\text{Li}_2\text{FeSiO}_4$ cannot be delithiated beyond the first Li in most experiments, and oxygen loss is avoided; whereas $\text{Li}_2\text{MnSiO}_4$ is usually fully delithiated and thus suffers from the structure degradation.

Li diffusion upon delithiation

Our analysis thus far is based primarily on thermodynamic considerations. When considering the impact of charge and discharge on a collapsed framework; however, kinetics can also be important. Accordingly, we have calculated Li migration barriers in the collapsed LiMnSiO_4 and MnSiO_4 structures *via* several possible diffusion paths, in comparison with that in the orthorhombic $\text{Li}_2\text{MnSiO}_4$ structure. Fig. 9 shows the preferred diffusion paths at different states of lithiation, with the corresponding migration barriers. Li diffuses along the *a*-axis during the charge process; the diffusion barriers in $\text{Li}_x\text{MnSiO}_4$ ($x = 2, 1, 0$) were calculated to be 0.87, 0.96, and 0.30 eV, respectively. These calculated high barriers indicate sluggish Li diffusivity within the material. In fact, $\text{Li}_2\text{MnSiO}_4$ is a poor Li conductor at room temperature; the electrochemical properties observed cannot be achieved unless the particles are made sufficiently small.

The Li diffusion barrier is only 0.09 eV higher in the collapsed framework of LiMnSiO_4 than that in $\text{Li}_2\text{MnSiO}_4$, which suggests that Li diffusion is not strongly hindered by the

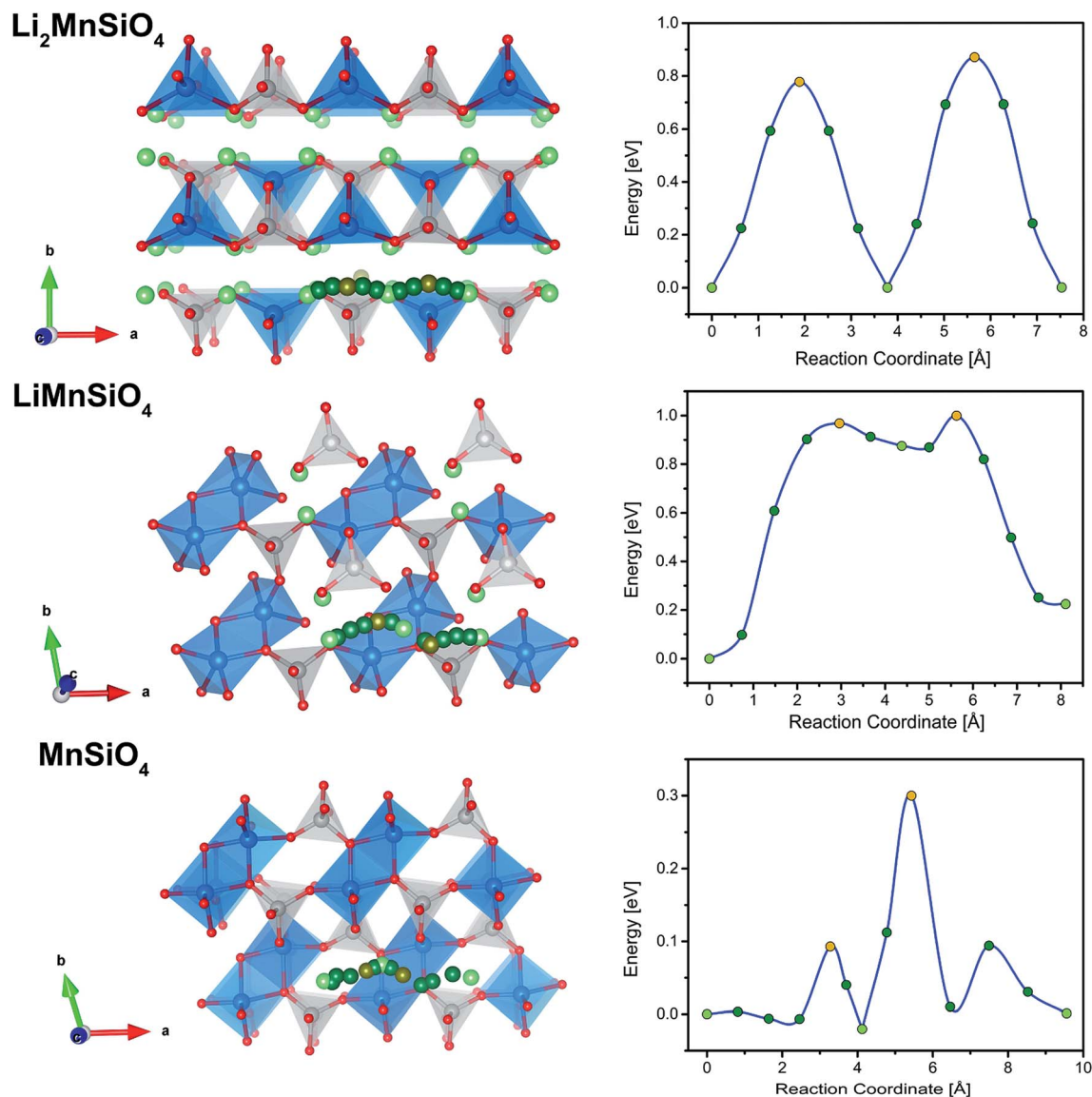


Fig. 9 Li ion diffusion paths in $\text{Li}_x\text{MnSiO}_4$ ($x = 2, 1, 0$) and the corresponding migration barriers. Light green, dark green and brown denote end-, intermediate-, and saddle-points, respectively.

structural collapse. Moreover, the diffusion barrier in MnSiO_4 is much lower than that in LiMnSiO_4 , and the only difference between them is the Li composition, indicating that Li diffusion is more sensitive to Li concentration than the structural framework. Therefore, by the reversibility calculated above and the facile diffusion shown here, we have demonstrated that the structural collapse is not the primary origin of the poor cyclability.

Conclusions

In summary, by performing DFT calculations, we find that the structural collapse in partially delithiated $\text{Li}_2\text{MnSiO}_4$, characterized by the transition from the MnO_4 tetrahedron to MnO_5 square pyramids, is reversible and does not impede Li intercalation. The reversibility of this structural collapse is confirmed

by cycling experiments. We show that the irreversible structural change in the first cycle is caused by oxygen evolution in the highly delithiated state. Moreover, the oxygen deficient structure can only intercalate the first Li when the discharge cutoff is 1.5 V; the second Li can only be inserted at a low voltage (0.4 V), which is not suitable for cathode materials. This oxygen evolution model explains the voltage profile shifts during the first few cycles and the limited discharge capacity of $\text{Li}_2\text{MnSiO}_4$. For comparison, the good cycle performance exhibited by $\text{Li}_2\text{FeSiO}_4$ is due to voltage limitations imposed on the extraction of the second Li, preventing oxygen evolution in the material.

This is the first time that the impact of oxygen evolution of highly charged $\text{Li}_2\text{MnSiO}_4$ and the explicit mechanism of structural change on the charge/discharge process is proposed, providing a new perspective for understanding the experimental behavior of $\text{Li}_2\text{MnSiO}_4$. Oxygen evolution appears to be

a common issue in layered oxide cathode materials, *i.e.* LiCoO₂, Li₂MnO₃ and other Li-rich compounds; extracting as much Li as possible without damaging the oxygen network is the essential issue for the stability of these cathode materials. Our results suggest that future research combining experiments and calculations will need to focus on stabilizing the oxygen network in highly charged states to overcome the primary limitations of Li₂MnSiO₄ as a Li ion cathode material.

Conflict of interest

The authors declare no competing financial interest.

Acknowledgements

This work was supported by the Welch Foundation under grant F-1841. Computational resources were provided by the Texas Advanced Computing Center. We greatly appreciate Professor John Goodenough, who has given us many helpful comments. Q. C. and Y. P. would like to thank the China Scholarship Council (CSC) for supporting their study as exchange students in UT Austin and U.W.

References

- 1 Y. S. Meng and M. E. Arroyo-de Dompablo, *Acc. Chem. Res.*, 2013, **46**, 1171.
- 2 Y. Zhao, C. Wu, J. Li and L. Guan, *J. Mater. Chem. A*, 2013, **1**, 3856.
- 3 V. Aravindan, K. Karthikeyan, S. Ravi, S. Amaresh, W. S. Kim and Y. S. Lee, *J. Mater. Chem.*, 2010, **20**, 7340.
- 4 H. Wang, T. Hou, D. Sun, X. Huang, H. He, Y. Tang and Y. Liu, *J. Power Sources*, 2014, **247**, 497.
- 5 F. Wang, J. Chen, C. Wang and B. Yi, *J. Electroanal. Chem.*, 2013, **688**, 123.
- 6 A. Bhaskar, M. Deepa, T. N. Rao and U. V. Varadaraju, *J. Electrochem. Soc.*, 2012, **159**, A1954.
- 7 A. Kokalj, R. Dominko, G. Mali, A. Meden, M. Gaberscek and J. Jamnik, *Chem. Mater.*, 2007, **19**, 3633.
- 8 B. Shao, Y. Abe and I. Taniguchi, *Powder Technol.*, 2013, **235**, 1.
- 9 M. E. Arroyo-de Dompablo, M. Armand, J. M. Tarascon and U. Amador, *Electrochem. Commun.*, 2006, **8**, 1292.
- 10 M. E. Arroyo-de Dompablo, R. Dominko, J. M. Gallardo-Amores, L. Dupont, G. Mali, H. Ehrenberg, J. Jamnik and E. Morán, *Chem. Mater.*, 2008, **20**, 5574.
- 11 S. Q. Wu, Z. Z. Zhu, Y. Yang and Z. F. Hou, *Comput. Mater. Sci.*, 2009, **44**, 1243.
- 12 P. Larsson, R. Ahuja, A. Liivat and J. O. Thomas, *Comput. Mater. Sci.*, 2010, **47**, 678.
- 13 G. Zhong, Y. Li, P. Yan, Z. Liu, M. Xie and H. Lin, *J. Phys. Chem. C*, 2010, **114**, 3693.
- 14 M. M. Kalantarian, S. Asgari and P. Mustarelli, *J. Mater. Chem. A*, 2013, **1**, 2847.
- 15 H. Lee, S. Park, J. Moon, H. Lee, K. Cho, M. Cho and S. Y. Kim, *Chem. Mater.*, 2014, **26**, 3896.
- 16 L. Li, L. Zhu, L. Xu, T. Cheng, W. Wang, X. Li and Q. Sui, *J. Mater. Chem. A*, 2014, **2**, 4251.
- 17 L. Zhu, L. Li, T. Cheng and D. Xu, *J. Mater. Chem. A*, 2015, **3**, 5449.
- 18 A. Saracibar, Z. Wang, K. J. Carroll, Y. S. Meng and M. E. Arroyo-de Dompablo, *J. Mater. Chem. A*, 2015, **3**, 6004.
- 19 N. Colligan, V. Augustyn and A. Manthiram, *J. Phys. Chem. C*, 2015, 123905380.
- 20 M. Moriya, M. Miyahara, M. Hokazono, H. Sasaki, A. Nemoto, S. Katayama, Y. Akimoto, S. Hirano and Y. Ren, *J. Power Sources*, 2014, **263**, 7.
- 21 H. Wang, T. Hou, D. Sun, X. Huang, H. He, Y. Tang and Y. Liu, *J. Power Sources*, 2014, **247**, 497.
- 22 M. Moriya, M. Miyahara, M. Hokazono, H. Sasaki, A. Nemoto, S. Katayama, Y. Akimoto and S.-i. Hirano, *J. Electrochem. Soc.*, 2014, A97.
- 23 P. Zhai, S. Zhao, H. Cheng, J. Zhao and C. Nan, *Electrochim. Acta*, 2015, **153**, 217.
- 24 V. Aravindan, K. Karthikeyan, K. S. Kang, W. S. Yoon, W. S. Kim and Y. S. Lee, *J. Mater. Chem.*, 2011, **14**, A33.
- 25 Y. Li, Z. Gong and Y. Yang, *J. Power Sources*, 2007, **174**, 528.
- 26 W. Liu, Y. Xu and R. Yang, *Rare Met.*, 2010, **29**, 511.
- 27 S. W. Lee, C. Carlton, M. Risch, Y. Surendranath, S. Chen, S. Furutsuki, A. Yamada, D. G. Nocera and Y. Shao-Horn, *J. Am. Chem. Soc.*, 2012, **134**, 16959.
- 28 J. B. Goodenough and K. Park, *J. Am. Chem. Soc.*, 2013, **135**, 1167.
- 29 R. Shunmugasundaram, R. Senthil Arumugam and J. R. Dahn, *Chem. Mater.*, 2015, **27**, 757.
- 30 P. Yan, L. Xiao, J. Zheng, Y. Zhou, Y. He, X. Zu, S. X. Mao, J. Xiao, F. Gao, J. Zhang and C. Wang, *Chem. Mater.*, 2015, **27**, 975.
- 31 A. R. Armstrong, M. Holzapfel, P. Novák, C. S. Johnson, S. Kang, M. M. Thackeray and P. G. Bruce, *J. Am. Chem. Soc.*, 2006, **128**, 8694.
- 32 A. R. Armstrong, N. Kuganathan, M. S. Islam and P. G. Bruce, *J. Am. Chem. Soc.*, 2011, **133**, 13031.
- 33 X. Lu, H. Wei, H. Chiu, R. Gauvin, P. Hovington, A. Guerfi, K. Zaghbi and G. P. Demopoulos, *Sci. Rep.*, 2015, **5**, 8599.
- 34 M. Li, L. Zhang, X. Yang, Y. Huang, H. Sun, S. Ni and H. Tao, *J. Solid State Electrochem.*, 2015, **19**, 415.
- 35 P. E. Blöchl, *Phys. Rev. B: Condens. Matter Mater. Phys.*, 1994, **50**, 17953.
- 36 W. Kohn, A. D. Becke and R. G. Parr, *J. Phys. Chem.*, 1996, **100**, 12974.
- 37 A. I. Liechtenstein, V. I. Anisimov and J. Zaanen, *Phys. Rev. B: Condens. Matter Mater. Phys.*, 1995, **52**, R5467.
- 38 D. Sheppard, P. Xiao, W. Chemelewski, D. D. Johnson and G. Henkelman, *J. Chem. Phys.*, 2012, **136**, 74103.
- 39 P. Xiao, J. Song, L. Wang, J. B. Goodenough and G. Henkelman, *Chem. Mater.*, 2015, **27**, 3763.
- 40 N. P. Wagner, P. E. Vullum, M. K. Nord, A. M. Svensson and F. Vullum-Bruer, *J. Phys. Chem. C*, 2016, **120**, 11359.
- 41 N. Wagner, A. M. Svensson and F. Vullum-Bruer, *Transl. Mater. Res.*, 2016, **3**, 25001.
- 42 L. Qu, S. Fang, L. Yang and S. Hirano, *J. Power Sources*, 2014, **252**, 169.

- 43 J. S. Hummelshøj, J. Blomqvist, S. Datta, T. Vegge, J. Rossmeisl, K. S. Thygesen, A. C. Luntz, K. W. Jacobsen and J. K. Nørskov, *J. Chem. Phys.*, 2010, **132**, 71101.
- 44 G. Ceder, *MRS Bull.*, 2010, **35**, 693.
- 45 R. Dominko, I. Arçon, A. Kodre, D. Hanžel and M. Gaberšček, *J. Power Sources*, 2009, **189**, 51.
- 46 K. Luo, M. R. Roberts, R. Hao, N. Guerrini, D. M. Pickup, Y. S. Liu, K. Edström, J. Guo, A. V. Chadwick and L. C. Duda, *Nat. Chem.*, 2016, **8**, 684.
- 47 E. Castel, E. J. Berg, M. E. Kazzi, P. Novák and C. Villevieille, *Chem. Mater.*, 2014, **26**, 5051.
- 48 M. Saubanère, E. McCalla, J. Tarascon and M. Doublet, *Energy Environ. Sci.*, 2016, **9**, 984.
- 49 Y. Pei, Q. Chen, C. Xu, H. Wang, H. Fang, C. Zhou, L. Zhen and G. Cao, *J. Mater. Chem. A*, 2016, **4**, 9447.
- 50 T. Masese, Y. Orikasa, C. Tassel, J. Kim, T. Minato, H. Arai, T. Mori, K. Yamamoto, Y. Kobayashi, H. Kageyama, Z. Ogumi and Y. Uchimoto, *Chem. Mater.*, 2014, **26**, 1380.
- 51 M. Armand and M. E. Arroyo Y De Dompablo, *J. Mater. Chem.*, 2011, **21**, 10026.
- 52 D. Lv, J. Bai, P. Zhang, S. Wu, Y. Li, W. Wen, Z. Jiang, J. Mi, Z. Zhu and Y. Yang, *Chem. Mater.*, 2013, **25**, 2014.